THE ASTROPHYSICAL JOURNAL, 422:351–365, 1994 February 10

THE CHROMOSPHERIC STRUCTURE OF THE COOL GIANT STAR g HERCULIS

DONALD G. LUTTERMOSER[1]
Iowa State University, Department of Physics & Astronomy, Ames, IA 50011
HOLLIS R. JOHNSON[2]
Indiana University, Astronomy Department, Bloomington, IN 47405
AND
JOEL A. EATON[1,2]
Tennessee State University, Center of Excellence in Information Systems, 330 10th Avenue North, Ste. 265, Nashville, TN 37203
Received 1992 November 16; accepted 1993 August 16

ABSTRACT

Non–LTE calculations of semiempirical chromospheric models are presented for 30 g Her (M6 III). This star is one of the coolest ($T_{\rm eff}$ = 3250 K) SRb (semiregular) variable stars and has a mass perhaps as great as 4 $M_\odot$. Chromospheric features we have observed in its spectrum include Mg II *h* and *k*; C II] UV0.01, which is sensitive to electron density; Mg I λ2852; Ca II H, K, and IRT; Ca I λ4227 and λ6573; Al II] UV1; and Hα. We pay special attention to fitting the C II intersystem lines and the Mg II resonance lines but use all the other features as constraints to some extent. The equations of radiative transfer and statistical equilibrium are solved self-consistently for H I, H^-, H_2, He I, C I, C II, Na I, Mg I, Mg II, Al I, Al II, Ca I, and Ca II with the equivalent two-level technique. To simplify these calculations, a one-dimensional hydrostatic, plane-parallel atmosphere is assumed.

We investigate 10 separate "classical" chromospheric models, differing most importantly in total mass column density above the temperature minimum. Synthetic spectra from these models fit some but not all of the observations. These comparisons are discussed in detail. However, we find that no single-component classical model in hydrostatic equilibrium is able to reproduce both the Mg II line profiles and the relative strengths of the C II] lines. In all these models, chromospheric emission features are formed relatively close to the star ($\lesssim 0.05 R_*$). The circumstellar environment has a thick, cool component overlying the Mg II emission region, which is relatively static and very turbulent. Finally, we find that thermalization in the Mg II *h* and *k* lines in the coolest giant stars is controlled by continuum absorption from Ca I $4p\,^3P^o$ bound-free opacity and not collisional de-excitation as is the case for warmer K giants.

Subject headings: stars: chromospheres — stars: individual (30 Herculis) — stars: late-type

1. INTRODUCTION

In contrast to photospheres, stellar chromospheres are regions where the temperature increases with height, attaining values in the range $T_{\rm eff} \lesssim T \lesssim 10{,}000$ K as the result of mechanical heating. Knowledge of the source of this mechanical heating in most stars is still preliminary in nature, but it is generally agreed that the heating probably depends on magnetic fields in main-sequence stars and giants earlier than ~K2 (e.g., Rutten 1987), while for cooler giants and supergiants, it may be accomplished by nonmagnetic processes (Middelkoop 1982; Schrijver 1987), for instance by long-period (perhaps in conjunction with short-period) acoustic waves (e.g., Bowen 1988; Cuntz & Stencel 1991; Ulmschneider 1991).

The chromospheres of cool stars reveal themselves through emission features of singly ionized and neutral metals in the violet and ultraviolet—especially the resonance lines of Mg II and Ca II. Mg II *h* and *k* show chromospheric emission to a greater degree than Ca II H and K because the higher abundance of ionized magnesium ensures a higher excitation rate, and because there is less photospheric continuum at the wavelength of Mg II than at Ca II in cool stars. Many lines of other common chemical elements are detected, too, although these tend to be weaker because of lower abundances (e.g., Al II), unfavorable excitation potentials (e.g., Si II), or complicated spectra which spread the emission over many lines (e.g., Fe II). Of particular importance is the C II] UV0.01 intersystem multiplet, whose line ratios are sensitive to electron density (Stencel et al. 1981), and the optically thin Al II] line at λ2669. Representative ultraviolet spectra of cool giants are given by Ayres et al. (1986) for α Boo (K1 III), Eaton & Johnson (1988) for several M giants, and Carpenter et al. (1988) for γ Cru (M3 III).

Studies to determine the mechanisms responsible for heating chromospheres are helped considerably with a detailed knowledge of the atmospheric structure of these layers. Two techniques have been used extensively in the past to estimate chromospheric conditions: (1) the empirical method, which estimates *global* characteristics of a chromosphere (e.g., Stencel et al. 1981; Brown & Carpenter 1984; Judge 1986a, b; Eaton & Johnson 1988), and (2) the semiempirical method, which attempts to constrain a model by fitting observed line strengths and profiles. Judge (1990) has argued that empirical techniques are often invalid because of the large range of column mass over which crucial chromospheric lines are formed. Should the lines in question be formed at slightly different depths, hence different densities and temperatures, it rapidly becomes unclear just what the global measures of physical properties represent.

The semiempirical technique leads to a detailed model of the atmospheric structure. In this procedure, a chromospheric

[1] Visiting Astronomer, National Solar Observatory, operated by the Association of Universities for Research in Astronomy, Inc., under cooperative agreement with the National Science Foundation.
[2] Guest Observer with the *International Ultraviolet Explorer*, operated by the National Aeronautics and Space Administration.

temperature-density stratification is attached to a radiative-equilibrium photospheric model appropriate for the star. The radiative transfer and statistical equilibrium equations are solved in a self-consistent way, and theoretical spectra are calculated. Such spectra are then compared with observations, and the differences between the two are used to decide how the model must be changed to fit the observations better. The chromospheric model is thus altered, and subsequent calculations made, until the synthetic spectra agree with the observed spectra. This technique has been applied to a few cool oxygen-rich giant stars. The coolest star of this type for which it has been used successfully is α Tau (Kelch et al. 1978), spectral type K5. Basri, Linsky, & Eriksson (1981) attempted to derive a model for the M2 supergiant α Ori with limited success, and, although not exactly semiempirically, Hartmann & Avrett (1984) also modeled the chromosphere of α Ori by adjusting the heating rate of hypothetical Alfvén waves until the chromospheric temperature structure could reproduce the observed spectrum of the Mg II resonance lines. TX Psc, an N0 irregular-variable carbon star, is the coolest giant for which a chromospheric model has been determined semiempirically (Luttermoser 1988; Luttermoser et al. 1989). Luttermoser & Johnson (1992) have recently discussed non–LTE (NLTE) effects in the ionization and excitation of hydrogen and helium in these very cool giant stars.

This paper represents the first attempt to form a detailed semiempirical model of the chromospheric structure of a cool ($T_{\rm eff} < 3500$ K), oxygen-rich giant star—specifically, g Her (M6 III). Such stars represent fertile new ground for chromospheric models in that the electron density and heating mechanisms may well be different than in warmer stars. In fact, line ratios within the C II] intersystem multiplets in g Her and 2 Cen both indicate electron densities about an order of magnitude lower than in K giants (Eaton & Johnson 1988). Such cool stars are usually variable, and pulsations are thought to contribute to heating the chromospheric gas (e.g., Bowen 1988; Cuntz & Stencel 1991; Eaton, Johnson, & Cadmus 1990). Indeed, it has been suggested that the structure of cool M giants may be quite different than that of K and warm M giants, with weaker chromospheres, much lower ionization of all elements, and extensive circumstellar dust formation (Stencel, Carpenter, & Hagen 1986). The mechanism of chromospheric heating, uncertain at present, may also be different in these cooler giants (Ulmschneider 1991; Dupree 1991; Cuntz & Stencel 1991).

Section 2 of this paper discusses the observations used for comparison with our theoretical models. Unlike the TX Psc model, which was based on fitting the noisy profile of only the Mg II *h* line and the integrated flux of C II] UV0.01, our model of g Her is derived from a multitude of high-resolution line profiles in the ultraviolet, optical, and infrared regions. Section 3 describes the procedure used in the NLTE calculations and applies them to g Her, while § 4 discusses the implications of the resulting model. We conclude the paper with § 5 by presenting the problems encountered with the modeling and summarizing possible solutions to the discrepancies between the synthetic and observed spectra.

2. OBSERVATIONS

The star 30 g Her (M6 III) is a semiregular (SRb) variable with $V = 5.04$ ($B-V = 1.52$, $U-B = 1.17$). Ultraviolet fluxes are barely bright enough for high-resolution, long-wavelength spectra with *IUE*, since the star is very inactive. The period of the star is listed as 89 days in the General Catalog of Variable Stars (Kukarkin et al. 1976), and robotic photometry over the last 6 yr shows changes in visual magnitude of ~0.3 mag on a period of roughly this length superposed on slower variations of close to 1.0 mag in *V* (Henry & Baliunas 1992). The visual spectrum is dominated by the typical TiO bands characterizing the M spectral type, but, unlike Mira variables, the star has never been reported to produce perceptible hydrogen-line emission at any phase. Its metallicity seems to be roughly solar, although carbon is depleted ty a factor of 2 with respect to iron (Smith & Lambert 1985). It has been suggested (Smith & Lambert 1985; Judge & Stencel 1991) that g Her is an AGB (asymptotic giant branch) star from its position in the H-R diagram, a possible slight enhancement of *s*-process elements, and its *IRAS* colors (i.e., AGB stars show evidence for dust; indeed, the *IRAS* LRS Spectral Atlas (Olnon & Raimond 1986) shows g Her to have weak dust features).

The semiempirical models described here are constrained by two high-resolution *IUE* spectra recording the line profiles of the C II] UV0.01 intersystem lines near 2325 Å, the Mg II *h* and *k* lines near 2800 Å, and the Mg I resonance line at 2852 Å. We have also used the overall appearance of an observed low-dispersion *IUE* spectrum to help constrain the angular size of the star from comparisons to the synthetic spectra. Table 1 lists the properties of the spectra used. The *IUE* data were reduced with the standard IUESPS software at NASA's Goddard Space Flight Center; we have calibrated them with the calibrations of Cassatella & Harris (1983) and Cassatella, Ponz, & Selvelli (1983). The integrated multiplet fluxes in these spectra were 6.6, 2.4, 71.8, and 2.5×10^{-13} ergs s^{-1} cm^{-2} for C II] UV0.01, Al II] UV1, Mg II UV1, and Mg I UV1, respectively. The *k*/*h* ratio for Mg II is 1.43, rather typical for K and M giants (Stencel et al. 1980). We have used LWP 13442 for the Mg II lines, since they were saturated in LWP 13443, and LWP 13443 for the weaker features, C II], Mg I, and Al II. Table 2 gives some useful measurements of the spectra. For the observations, we have listed integrated flux at the Earth in the Mg II

TABLE 1

SUMMARY OF g HER CULIS OBSERVATIONS

Wavelengths	Date (U.T.)	Telescope	Camera Sequenge	Resolving Power $\lambda/\Delta\lambda$	Exposure Time (minutes)
2500–3200 Å.....	1988 June 16	*IUE*	LWP 13441	500	5
2500–2900 Å.....	1988 June 16	*IUE*	LWP 13442	10,000	40
2300–3100 Å.....	1988 June 17	*IUE*	LWP 13443	10,000	880
3922–3975 Å.....	1989 Aug 13	McMath	SCCD 530	21,000	150
8488–8590 Å.....	1989 Aug 14	McMath	SCCD 547	23,000	2
4181–4248 Å.....	1989 Aug 27	McMath	SCCD 538	21,000	2
6540–6600 Å.....	1992 Apr 20	McMath	SCCD 517	45,000	5

TABLE 2

INTEGRATED FLUXES IN EMISSION LINES[a]

Line	Observed[b]	T2	T3	T4	T5	T6	T7	T8	T9	T10
Mg II *h* and *k*	7.2E − 12	...	896.	713.	6.96E3	1.3E5	5.89E6	7.2E4	8.05E3	1.99E4
C II λ2324.....	1.1E − 13	2.61	9.99	33.2	45.0	306.	7.86E4	292.	39.9	152.
C II λ2325.....	3.1E − 13	4.75	41.9	182.	240.	1.58E3	1.60E5	1.60E3	215.	879.
C II λ2327.....	1.6E − 13	3.65	22.9	88.3	124.	637.	6.37E4	664.	112.	423.
C II λ2328.....	8.6E − 14	2.69	10.3	34.5	46.8	318.	8.04E4	302.	41.5	158.
Line Ratios[c]										
C II/Mg II	0.092	...	1.02	0.498	0.068	0.069	0.067	0.039	0.053	0.084
Al II/Mg II	0.033	[d]	[d]	[d]	[d]	0.024	0.021	0.025	0.023	0.034
Mg II (*k*/*h*)	1.43	...	1.94	3.46	1.83	1.79	1.49	1.83	1.88	1.79
Mg I/Mg II	0.035	...	...	...	0.045	0.023	0.050	0.028	0.038	0.029
Ca I/Hα[e].....	1.12	0.017	0.017	0.017	0.041	[d]	12.	0.059	0.031	0.72

[a] Integrated fluxes in ergs s^{-1} cm^{-2}. An absorption line is indicated with ellipses (note that all the lines for model T1 were in absorption). Also note that all fluxes for T1 through T4 are determined under the assumption of CRD. For T5–T10, resonance line fluxes are calculated with PRD.

[b] Divide this column by $(5.876 \times 10^{-18})\alpha_*^2$, where α_* is the angular diameter of the star in milliarsec, to convert observed fluxes to model fluxes.

[c] C II] ≡ C II] UV0.01; Mg II ≡ Mg II *h* and *k*; Ca II ≡ Ca II H and K; Ca I ≡ Ca I λ6573.

[d] Line not calculated for this model.

[e] Ratio between the line center fluxes of these absorption lines. For model T10, this ratio gives 0.052 (no Kurucz opacities), 0.48 (Kurucz opacities included), and 0.72 (Kurucz + McMath convolution).

h and *k* lines, the flux at the Earth in the lines of the C II intersystem multiplet, and the ratios of fluxes in other emission lines to Mg II. The emission-line fluxes for the resonance transitions listed represent the chromospheric portion of the line (i.e., the "emission cores"). For the theoretical models, we give astrophysical flux at the star, along with the same ratios.

We have supplemented the *IUE* spectra with ground-based data obtained with the McMath telescope on Kitt Peak, Arizona. The main features observed were the Ca II lines (K and H at 3934 Å and 3968 Å, respectively, and the two IR triplet lines at 8490 Å and 8600 Å). Ca I λ4227 was observed at roughly the same time as well, and we have since added a spectrum at Hα. The spectra were placed on a heliocentric wavelength scale determined from observations of a calibration lamp, and calibrated with respect to the flux-reference star ϵ Aqr. The wavelength scale is accurate to ±2 km s^{-1}. Uncertainties in the flux calibration range between 10% and 25%. The theoretical signal-to-noise ratio (S/N) of the TI-4 chip (Jaksha 1989) is approximately 70 in the cores of the Ca II resonance lines and 150 at peak flux levels in this spectral region, while S/N is 100 in the cores of the IR triplet and 150 at peak flux levels. Table 1 summarizes these ground-based observations which were reduced with standard techniques using software developed by the authors (e.g., Luttermoser 1993). The only prominent feature of hydrogen that we have been able to observe is Hα. The region of Hα is full of molecular lines, but Hα has the shape and strength typical of M5–M6 giants, and Ca I λ6573 is also similar to other M5–M6 giants we have observed.

Perhaps the most uncertain observational characteristic of g Her is its angular diameter, which sets the scale of observed flux at the star. Neither the distance nor the stellar radius is accurately known, and the star cannot be analyzed by lunar occultation. In a compilation of characteristics of AGB stars, Judge & Stencel (1991) list g Her as lying at a distance of 250 pc, and having a radius of 630 $R_\odot$, a mass of 4.0 $M_\odot$, log $g = -0.6$, an effective temperature of 3250 K, and an angular diameter of 23.7 milliarcsec (mas). These values are quite conventional. Smith & Lambert (1985), for instance, give the same values of mass and effective temperature, although their gravity is much higher. Scargle & Strecker (1979) derived an angular diameter of 18.4 mas from a comparison between observed infrared fluxes and synthetic fluxes from a grid of late-type giant star fluxes published by Johnson (1974). This angular size is suspect however, since molecular opacities used in the models of Johnson (1974) were calculated with *straight means*, which will greatly reduce the flux in the frequency band where the straight mean is used. Indeed, Scargle & Strecker (1979) deduce an effective temperature for g Her of 3450 K, which is 200 K larger than the value determined by Smith & Lambert (1985). Scargle & Strecker also deduce an interstellar reddening to g Her of $E(B-V) = 0.53$, which we feel is too high for an M6 star whose color is $B-V = 1.52$. We suspect such a high value arose from errors introduced by their flux-comparison technique.

Figure 1 compares a synthetic spectrum generated with PANDORA for a purely photospheric model representative of

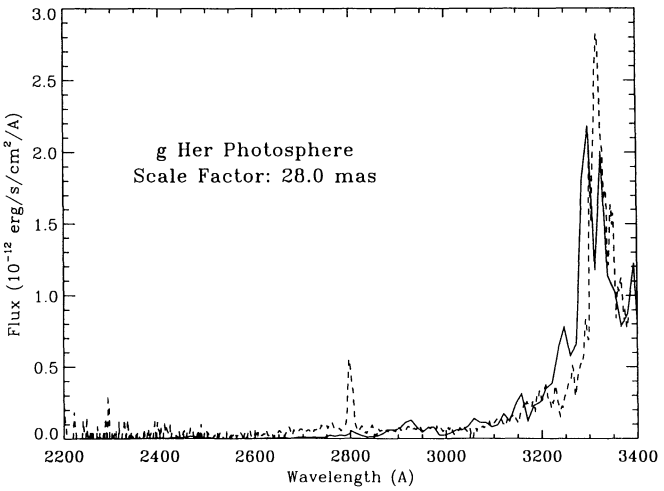

FIG. 1.—A comparison between the low-resolution *IUE* spectrum of g Her (LWP 13441) and a PANDORA synthetic spectrum of a "pure" photospheric model representative of g Her. The best fit is obtained when the synthetic spectrum is scaled to an angular diameter of 28.0 mas.

g Her with the "continuum" flux in a low-resolution *IUE* spectrum. The synthetic flux uses a compilation of bound-bound opacities described by Avrett, Machado, & Loeser (1986) which are based upon the line list of Kurucz & Peytremann (1975). It has been noted by Malagnini et al. (1992) that synthetic spectra based upon these older Kurucz line data reproduce the ultraviolet flux of cool stars better than the recent Kurucz line data. As a further check of the angular size of g Her, we altered the synthetic flux scale factor of our photospheric model until a best fit was obtained via a minimization of the residuals between the observed and synthetic fluxes. This fit gives an angular diameter of 28.0 mas and we have used this scale factor for our first attempts at fitting the profiles. Finally, all synthetic spectra are shifted in wavelength by the photospheric radial velocity of 3 km s^{-1} (Hoffleit 1982) for comparison with observations.

3. RADIATIVE TRANSFER CALCULATIONS

In constructing the chromospheric models, we followed the technique described by Luttermoser et al. (1989). First we obtain the plane-parallel, radiative-equilibrium model photosphere from the "Indiana-grid" of atmospheres with the closest match to the characteristics of g Her. For this study, we selected a model with solar abundance, $T_{\rm eff} = 3200$ K, and $g = 1$ cm s^{-2} from Brown et al. (1989). Since this photospheric model extends up only to a column mass m of 6.4×10^{-2} g cm^{-2}, where the resonance lines of interest would still be very optically thick, we first extend the model out to a column mass of approximately 10^{-14} g cm^{-2} (see Luttermoser & Johnson 1992). Note here that we did *not* reconverge this extended photospheric model under the assumption of radiative equilibrium; we merely *extrapolated* the temperature-density gradient from the top of the published model. A synthetic spectrum calculated for this model was then used to set the flux scale factor between the observed and synthetic spectra, hence angular size of the star (see Fig. 1). We then increased the temperature as a function of height at an arbitrary depth in this extended photosphere to simulate a chromosphere. For all these calculations, we initially assumed a low microturbulent velocity of 3 km s^{-1} throughout the atmosphere, roughly the photospheric value (Smith & Lambert 1985; Tsuji 1991).

Because the ionization and excitation in chromospheric gases may depart wildly from the predictions of LTE (local thermodynamic equilibrium), a self-consistent solution to the coupled equations of statistical equilibrium and radiative transfer are required for a model atom of the species to be considered. These calculations were performed with the radiative transfer code PANDORA (e.g., Vernazza, Avrett, & Loeser 1973 [VAL I], 1978 [VAL II], 1981 [VAL III]; Avrett & Loeser 1992) in a horizontally homogeneous, plane-parallel geometry. Under these assumptions, the radiative transfer equation is written as

$$\mu \frac{dI_\nu}{d\tau_\nu} = I_\nu - S_\nu \,, \tag{1}$$

where parameters above have their usual meaning, and the quantities shown include all processes (continuum and line) taking place at that frequency. Statistical equilibrium is formulated as

$$n_i \sum_{j=1(\neq i)}^{N} (P_{ij} + P_{i\kappa}) = \sum_{j=1(\neq i)}^{N} (n_j P_{ji} + n_\kappa P_{\kappa i}) \,, \tag{2}$$

and

$$n_\kappa \sum_{i=1}^{N} P_{\kappa i} = \sum_{i=1}^{N} n_i P_{i\kappa} \,, \tag{3}$$

where n_i represents the number density in bound level i (up to a maximum of N levels in the representative atomic model), n_κ represents the continuum (i.e., ion) number density, and P represents the total transition rate (radiative R plus collisional C) between the respective states. Equations (1)–(3) are solved iteratively with the equivalent two-level approach. With this method, emission and absorption of photons in a line are expressed in terms of a net radiative bracket ρ_{ji} defined by the net radiative rate equation

$$n_j A_{ji} \rho_{ji} = n_j (A_{ji} + B_{ji} \bar{J}_{ji}) - n_i B_{ij} \bar{J}_{ji} \,, \tag{4}$$

where A_{ji}, B_{ji}, and B_{ij} are the Einstein coefficients for spontaneous emission, stimulated emission, and absorption respectively, and $\bar{J}$ is the total mean intensity integrated over the normalized absorption coefficient in the ji transition. It can be shown that the line source function can be written as

$$S_{ji} = \frac{2h\nu_{ji}^3/c^2}{(g_j/g_i)(n_i/n_j) - 1} \,, \tag{5}$$

and the net radiative bracket as

$$\rho_{ji} = 1 - \frac{\bar{J}_{ji}}{S_{ji}} \,, \tag{6}$$

where g represents the statistical weight of the level.

We assume that the pressure is described by the equation of hydrostatic equilibrium and total particle density by the ideal gas law. Since the equations and techniques used in PANDORA are well documented in VAL I, II, III, and Avrett & Loeser (1992), and the specific techniques used here are described in Luttermoser et al. (1989) and Luttermoser & Johnson (1992), we shall present only relevant additions that are used in this work. For each chromospheric model, we iteratively solve the equations mentioned above for the following atomic models: H I (3-level), He I (5-level), C I (10-level), C II (7-level), Na I (8-level), Mg I (7-level), Mg II (6-level), Al I (6-level), Al II (3-level), Ca I (8-level), and Ca II (5-level). All other species are handled in LTE. All of these atomic models except Al I and Al II have been described in the references listed above. The six levels included in the Al I model are: (1) $3p\,^2P^o$, (2) $4s\,^2S$, (3) $3p^2\,^4P$, (4) $3d\,^2D$, (5) $4p\,^2P^o$, and an autoionization state (6) $3p^2\,^2S$, and four radiative bound-bound transitions: 2–1 (λ3944.0), 4–1 (λ3082.2), 5–2 (λ13123.4), and the dielectronic recombination transition 6–1 (λ1930.9). The Al II model includes the following levels: (1) $3s^2\,^1S$, (2) $3p\,^3P^o$, and (3) $3p\,^1P^o$, and two radiative bound-bound transitions: 2–1 (λ2669.2) and 3–1 (λ1670.8).

All bound-bound transitions are first assumed to be in *complete redistribution* (CRD). Upon the convergence of the CRD runs, we then compute the following lines in *partial redistribution* (PRD): H I Lyα, Mg I λ2852, Mg II λ2796, λ2803, Ca I λ4227, and Ca II λ3934, λ3968. We use the partial coherent scattering (PCS) approximation for PRD as described Avrett & Loeser (1984) and include Doppler diffusion in the line wings via the technique described by Hubený (1985). Gayley (1992) has shown that this approximation should be a valid description of PRD in cool, giant-star chromospheres for the Mg II h and k and the Ca II H and K lines. Luttermoser & Johnson (1992) have shown that the Lyα line (actually the line wings)

controls the ionization of hydrogen in this model. PRD effects in Lyα have a significant impact on the hydrogen ionization and excitation equilibrium in the temperature minimum region, since the extreme line wings are formed there and control much of the transfer of the line. The assumption of PRD in Lyα gives a factor of 2 increase in the proton density in the temperature minimum region as compared to the assumption of CRD. However, hydrogen is a negligible contributor to the electron density in this region (magnesium electrons dominate), so the factor of 2 increase of hydrogen electrons from PRD is insignificant to the structure of the atmosphere.

We calculated the line profiles for 10 separate chromospheric temperature distributions resembling "classical" chromospheric models—a rapid rise in temperature at the top of the photosphere followed by a linear increase in temperature as a function of column mass to some maximum value near 10,000 K at the top of the chromosphere. The temperature profiles for seven (T1, T3, T5, T6, T7, T8, and T10) of the representative models are plotted in Figure 2. Properties of all 10 models are given in Table 3. Our first chromosphere (T1) introduced a temperature rise at $T = 2119$ K and log $m = -1.23$ (or $z = -1.52 \times 10^7$ km, where z increases into the star, and $z = 0$ corresponds to $\tau[5000\ \text{Å}] = 1$) with a linear temperature increase with respect to log m up to the top of the model, where $T = 12{,}000$ K at log $m = -13.9$ ($z = -1.85 \times 10^8$ km). This model was unsatisfactory in that it produced pure absorption features for Mg I UV1, Mg II h and k, Ca II H and K, and C II] UV0.01. We next enhanced the temperature in the lower chromosphere ($-9.34 <$ log $m < -1.68$ [g cm^{-2}] or $-1.02 \times 10^8 < z < -1.70 \times 10^7$ km) by an average of 1000 K (chromosphere T2). The temperature enhancement at the base of the chromosphere increased the pressure scale height, which in turn expanded the top of the chromospheric model out to -2.21×10^8 km. This model produced weak C II] features with an integrated flux at Earth of 1.6×10^{-14} ergs s^{-1} cm^{-2} (for an angular diameter of 28 mas). Our resonance lines of interest remained pure absorption features, however.

We then moved the temperature minimum inward by 1.2×10^6 km (to log $m = -0.92$, $T = 2140$ K) and further enhanced the lower chromospheric temperature (chromosphere T3). This further increased the C II] flux and finally produced emission in the cores of the Mg II h and k lines. Similar, weaker, emission components were seen in Ca II H and K, yet Mg I UV1 remained a pure absorption feature. It has been shown by Luttermoser et al. (1989) that the Mg I UV1 emission will form in roughly the same chromospheric region that produces most of the Mg II and C II] line emission. We may thus improve the model by identifying the depth at which the Mg II emission features form and increase the temperature there to give the Mg I emission.

Chromosphere T5 finally produced an emission feature in Mg I UV1, so we use this model to take a detailed look at the line profiles. Figure 3 displays the Mg II lines calculated in PRD in a static atmosphere and compares them with the *IUE* observations. We had to scale the angular size of the model to 18.4 mas for the best fit, well within the uncertainties of the angular diameter of g Her. The overlying absorption due to Mn I UV1 and Fe I UV3 is obvious on the shortward side of the k line. Although not prominent in this spectrum, Fe I UV3 also hides some of the emission on the longward side of the h line. One problem with this fit is that the synthetic profiles are too broad at the base. There are several possible reasons for this. (1) Our chromosphere may be slightly too hot at the depth these photons are formed, thereby giving too much emission. (2) The scheme for calculating partial redistribution (i.e., PCS approximation with the Hubený description of Doppler diffusion in the line wings—*depth-dependent* PCS) may be inadequate. In these models, the base of the emission features of Mg II are formed in the upper photosphere, below the temperature minimum, from photons that have scattered downward from the chromosphere. If photons do not diffuse back toward line center, as they are assumed to do in the Hubený formulation, the escape probability is much higher than assumed in the wings, and photons are more likely to escape than to scatter downward. This would produce a narrower line, without the broad shallow wings. Figure 4 displays depth of formation information for the "core" (i.e., inner 2 Å) of the k line for $\mu = 0.5$, which represents the angle where the

TABLE 3

CHROMOSPHERIC MODELS CONSIDERED

Model	T_{min}[a]	log m_{min}[a]	T_{knee}[b]	log m_{knee}[b]	n_e(C II])[c]	H (km)[d]
T1	2119	−1.23	...	...	...	1.70×10^8
T2	2119	−1.23	3500	−1.68	2.9×10^6	2.06×10^8
T3	2140	−0.92	5500	−2.28	9.3×10^6	2.21×10^8
T4	2140	−0.92	6200	−2.28	8.9×10^6	2.31×10^8
T5	2156	−0.70	6800	−2.28	1.6×10^7	2.35×10^8
T6	2264	−0.03	5800	−1.23	9.1×10^6	1.67×10^8
T7	2426	0.68	6920	−1.23	1.2×10^9	2.16×10^8
T8	2223	−0.25	6200	−1.68	9.1×10^7	2.02×10^8
T9	2156	−0.70	6800	−2.28	1.4×10^7	2.45×10^8
T10.....	2156	−0.70	7000	−2.28	3.4×10^7	2.23×10^8

[a] Temperature (in K) and the logarithm of the column mass (in g cm^{-2}) of the atmospheric position that separates the photosphere from the chromosphere.

[b] Temperature (in K) and the logarithm of the column mass (in g cm^{-2}) of the atmospheric position where the chromospheric temperature profile flattens.

[c] Electron density (in cm^{-3}) at the depth of formation of the C II] UV0.01 features.

[d] Thickness of the chromosphere (in km) from the temperature minimum to the outermost region.

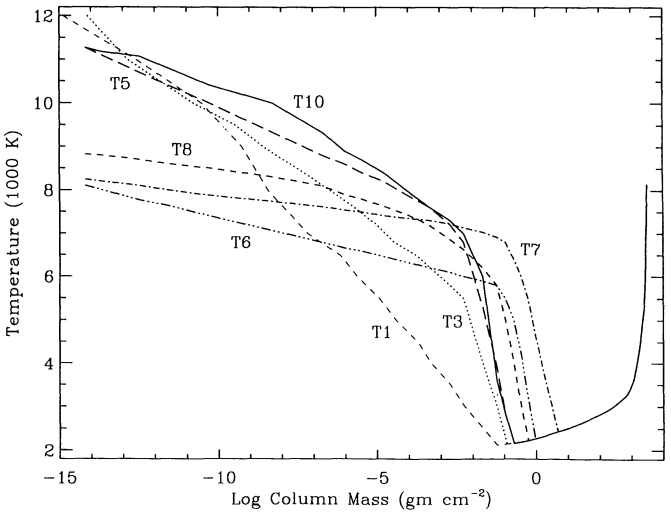

FIG. 2.—Temperature rises of representative chromospheric models. Temperature is displayed as a function of mass column density for models T1, T3, T5, T6, T7, T8, and T10. Note that model T10 is our final representative, one-dimensional chromosphere of g Her.

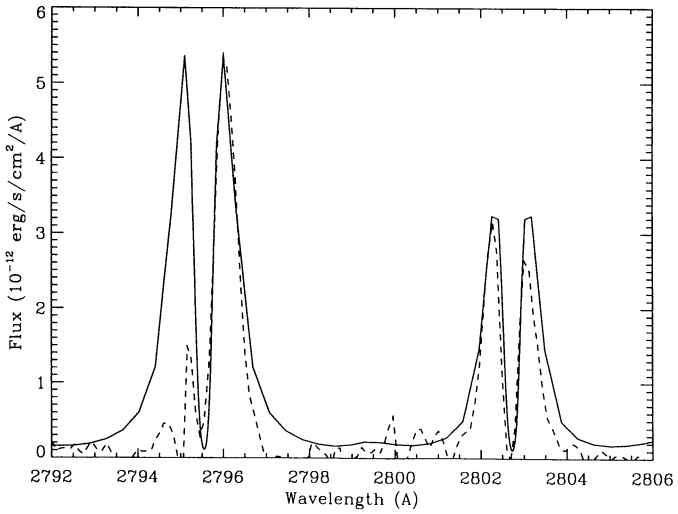

FIG. 3.—The Mg II *k* and *h* lines calculated in PRD in a static atmosphere (*solid*) compared with the high-dispersion *IUE* spectrum LWP 13442 (*dashed*). The synthetic flux is scaled to an angular diameter of 18.4 mas and convolved with a 0.17 Å FWHM Gaussian profile representative of the LWP camera at this dispersion (Evans & Imhoff 1985). The observed spectrum is displayed in heliocentric wavelength, and the synthetic spectrum has been shifted by +3 km s^{-1}, the photospheric radial velocity of g Her. Note that overlying absorption from Mn I (2794.82 Å) and Fe I (2795.01 Å, 2803.16 Å) corrupts the Mg II profiles.

maximum intensity occurs. One can see from this figure immediately that the inner 2 Å of the Mg II lines form over eight orders of magnitude in column mass! The emission portion of the core alone forms over four orders of magnitude in column mass. The peak flux of these lines originates at a column mass of 2.10×10^{-2} g cm^{-2}. By comparing these figures with Figure 3 (the line flux profile) and Figure 2 (the temperature structure), one can see that the base of the emission originates in the photosphere just below the temperature minimum region. This eliminates possibility (1) above.

The analysis of the validity of the depth-dependent form of PCS depends upon the mechanism that dominates the thermalization length at the depth of formation of the emission features. The thermalization length of the Mg II *k* line for collisional de-excitation at the depth of formation of the peak flux is approximately a factor of 70 larger than that for continuum absorption. Thus the thermalization in the line wings of the Mg II resonance lines is controlled by *continuum processes* (see Hubený 1985). This results mainly from the strong Ca I bound-free opacity from the 4p $^3P^o$ metastable state which suggests that the thermalization properties of the Mg II lines in cool M, S, and N (i.e., carbon) stars are fundamentally different than the warmer K stars. In contrast to the thermalization length, Hubený defines the *frequency thermalization length* as the highest frequency into the wing x (in units of Doppler widths) for which a photon has a substantial chance of becoming frequency-thermalized, i.e., it can suffer a sufficient number of scatterings to be removed from the wing to the line core before escaping from the medium. Processes through which it is lost from the core have different characteristic thermalization lengths. If one compares the frequency thermalization length, neglecting microturbulence for the time being, for the line scatterings (x_l) and the overlapping continuum (x_c) at the depth of formation of the emission peak for the *k* line, $x_l = 14$ and $x_c = 7$ Doppler widths. As such, the continuum processes dominate in the "emission wings" and Doppler diffusion is negligible there (see Hubený 1985 for further discussion). The depth-independent PCS formalism should then reproduce the redistribution function better than the depth-dependent formalism. We shall test this later in the paper.

Figure 5 displays a comparison between the synthetic and observed spectra in the C II] UV0.01 spectral region. Note that the angular size of the model had to be scaled down to 8.8 mas to achieve the fit with model T5. This is equivalent to reducing the abundance of carbon relative to magnesium by a factor of 4, while the measured abundances (Smith & Lambert 1985) suggest the carbon should be merely *halved*. It is clear from this comparison that the calculated spectrum is wrong in other ways as well. The lines near 2324.7 and 2328.2 Å are relatively much weaker in the synthetic spectrum than in the observation. Stencel et al. (1981) and Lennon et al. (1985) have shown

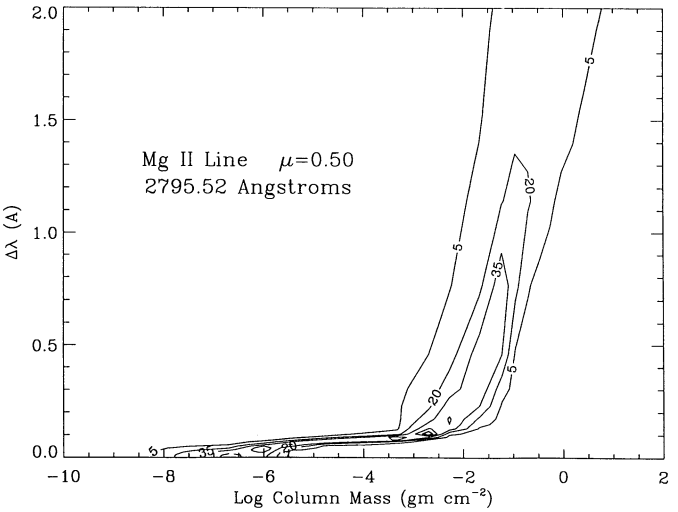

FIG. 4.—The depth of formation, or contribution function, of the Mg II *k* line expressed in percentages (5%, 20%, 35%, 50%, and 65%) at $\mu = 0.5$. Note that the extreme portion of the emission feature originates in the upper photosphere from chromospheric photons scattering out to this region of the line profile (see text).

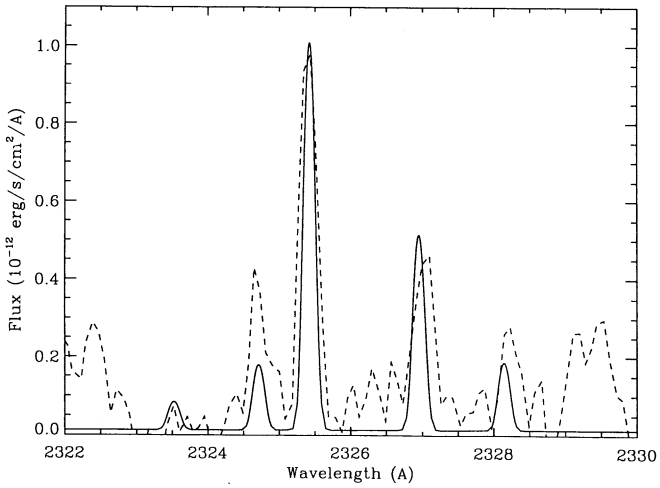

FIG. 5.—Synthetic (*solid*) and observed (*dashed*) spectra compared in the C II] UV0.01 spectral region. The synthetic flux, convolved with a Gaussian with a FWHM of 0.13 Å (Evans & Imhoff 1985), is scaled to 8.8 mas to achieve the best fit to the λ2325.40 line, which is equivalent to reducing the carbon abundance by a factor of 4.

that the line flux ratios of the intersystem multiplet are strongly sensitive to electron density over a range of $10^7 < n_e < 10^{10}$ cm^{-3}. These discrepancies in the line ratios are consistent with an error in density. In this model the electron density at the depth of formation of the C II] lines is 1.6×10^7 cm^{-3}. The observed ratio of the λ2324.69 line to the λ2326.93 line (the R_3 ratio of Lennon et al.) indicates it should be $n_e \sim 4 \times 10^8$ cm^{-3}. This is lower than the densities deduced for K giants, and the observed line ratios reflect it. Although the λ2326.93 line is blended with Fe II UV3 at 2327.39 Å in some of the K giants, this Fe II feature seems to weaken in the M stars and is probably unimportant in g Her, where the separation of line centers is as great as the breadth of the C II] lines, yet no feature is obvious at the rest wavelength of Fe II. In a similar way, the C II] line at 2328.12 Å would be blended with Si II] λ2328.51. Judge, Carpenter, & Harper (1991) have calculated spectra for α Tau, finding the Si II] line is only a few percent as strong as the C II] line. While these questions of blending add uncertainty to the derived values of electron density, they are no worse than those caused by the noise of the spectrum. Even so, the measured ratios of lines in the C II] multiplet $R_1 \geq 3.5$, $R_2 = 1.1$, and $R_3 = 0.9$, lead to an electron density of 1–6×10^8 cm^{-3} on the scale of Lennon et al. (1985) in this region of the chromosphere. Finally, the synthetic spectrum of C II] indicates that the assumption of 3 km s^{-1} may be too low, since the width of the lines are smaller than the observations (see also Judge 1986a, b; Carpenter et al. 1991).

We next constructed two additional chromospheric structures, T6 and T7 (see Fig. 2), with which we tried to reproduce the C II] flux ratios. To obtain sufficiently high values of electron density in the emission region with a conventional model, we were forced to push the chromospheric temperature rise inward. Indeed, we could match the flux ratios of the C II] multiplet more closely with model T7 than with T6 or T5, but this model's greater mass and larger optical depth made the Mg II emission lines much too broad (i.e., the Wilson-Bappu or Weiler-Oegerle effect). More telling, it forced Mg I λ4571 into emission in T6 as well as in T7, contrary to the observations of M giants. There was also a problem for Hα, which became a very broad, deep absorption line in model T7. This simply means that the optical depth of Hα was too great in the chromosphere of the more massive models. In fact, if we artificially increase the electron density to $\sim 2 \times 10^8$ cm^{-3} throughout the chromosphere, we get about the right strength of Hα with the relatively low-mass model T8, but this model is bad because the emission features in Mg I and Ca II H and K were much too strong in comparison to the observations.

Given the great discrepancy in electron density and our inability to account for it by increasing the chromosphere's depth, we conclude that it is *impossible* to reproduce both the Mg II and C II] features (all formed in roughly the same region of the chromosphere) with a *classical one-dimensional, static, hydrostatic atmosphere.* Because of the small ratio of atmospheric thickness to stellar radius at the formation depths of these emission features ($\sim$1%), effects of sphericity are expected to be small. This expectation is borne out by a comparison of the temperature-pressure structure in our models with those from a recent grid of models with spherical geometry and OS (opacity sampling) opacities (Plez, Brett, & Nordlund 1992), where temperature differences in layers above the region of continuum emission are generally smaller than 30 K, and even this slight difference is probably due more to different opacities than to the plane-parallel assumption. Synthetic spectra (from a model with $T_{\rm eff}/\log g = 3250/0.01$) agree well with the observations of g Her in the infrared region though the fit is slightly worse in the visual and ultraviolet regions. We note that the parameters chosen for g Her by these workers agree well with the values employed in the present work (3200/0.0).

Under these circumstances, we have chosen to base our best *classical* chromosphere on the available resonance features, with the greatest weight given to Mg II *h* and *k*. The final model based on these criteria is T10 (Table 4). This model is quite similar to T5 and either model could be considered the final model. In fact, the model atmosphere use for g Her in the Luttermoser & Johnson (1992) paper was model T5. As in model T5, the Mg II profiles from the depth-dependent PCS approximation are too broad at the base of the emission line. We discovered that the best fit was obtained for depth-independent PCS with a CRD width $x_{\rm CRD}$ of 8 Doppler widths. This is consistent with the earlier finding that the frequency thermalization length is controlled by continuum absorption and is approximately 7 Doppler widths. The same problem exists for the line ratios of this multiplet as existed for model T5. Also, the C II] UV0.01 lines in model T10 display narrower lines than are observed for the initial guess of 3 km s^{-1} microturbulent velocity in the chromosphere. We carried out a series of calculations where the microturbulent velocity ξ is varied and found the best fit of the C II] UV0.01 widths resulted with $\xi = 20$ km s^{-1} in the chromosphere. We then went back and recalculated the Mg II profiles with this chromospheric microturbulence, with a depth-independent PCS (8 Doppler widths), which resulted in enormously broadened emission wings and self-reversed core due to the increased Doppler width from the large microturbulence. After trying a variety of microturbulence values at various depths in the chromosphere, we finally selected $\xi = 10$ km s^{-1} at the depth of formation of the peak flux of the Mg II and C II] emission ($m = 2.10 \times 10^{-2}$ g cm^{-2}) and $\xi = 15$ km s^{-1} at the depth just below ($m = 5.90 \times 10^{-2}$ g cm^{-2}), and let ξ quickly fall to 2 km s^{-1} for depths above and below this region. To achieve a good fit between the Mg II synthetic profiles and the observations, we needed to reduce the value of $x_{\rm CRD}$ of the depth-independent PCS to 3 Doppler widths. Although this CRD width is a factor of 2 less than the value of x_c (continuum frequency thermalization length) found earlier, we remind the reader that the earlier x_c estimation ignored microturbulence in the Doppler width calculation. Since x_c scales as $\Delta v_{\rm D}^{-1/4}$, an increase in the Doppler width due to microturbulence will result in a decrease in x_c. Figure 6 shows the resulting Mg II profiles for this choice of the microturbulent velocity and PCS parameter in a static model. Figure 7 shows the resulting C II] UV0.01 profiles. As can be seen, the widths of the C II] are still slightly narrower than the observations. Because the Mg II emission and the C II] lines are formed at essentially the same depth in the model, we can find no microturbulent value that is consistent with both of these features. The values listed above for the microturbulence are 2–3 times the adiabatic sound speed at the depths assigned these values, which further indicates that the one-dimensional, plane-parallel, hydrostatic equilibrium model is not valid for this star.

We next make a comparison between the observations and calculations of the Mg I resonance line for model T10. As is the case for Mg II, the calculated Mg I emission profile is too broad at the base of the feature for the depth-dependent PCS. Furthermore, the Mg I emission feature is formed at the same depth as the Mg II features and this line lies even closer to the

TABLE 4

MODEL ATMOSPHERE T10 FOR g HERCULIS

Depth (km)	Temperature (K)	Column Density (g cm^{-2})	Total Pressure (dyne cm^{-2})	Hydrogen Density (cm^{-3})	Electron Density (cm^{-3})	Proton Density (cm^{-3})
−2.61E+08.....	11270.	6.53E−15	6.53E−15	1.93E−03	2.07E−03	1.93E−03
−2.45E+08.....	11180.	1.98E−14	1.98E−14	6.03E−03	6.18E−03	6.03E−03
−2.07E+08.....	11070.	3.26E−13	3.26E−13	1.02E−01	1.02E−01	1.01E−01
−1.79E+08.....	10800.	2.57E−12	2.57E−12	8.33E−01	8.07E−01	8.05E−01
−1.43E+08.....	10410.	5.14E−11	5.14E−11	2.06E+01	1.31E+01	1.31E+01
−1.03E+08.....	10000.	5.38E−09	5.38E−09	3.29E+03	2.74E+02	2.69E+02
−7.94E+07.....	9330.	2.00E−07	2.00E−07	1.38E+05	3.33E+03	3.10E+03
−6.98E+07.....	8900.	9.99E−07	9.99E−07	7.27E+05	1.32E+04	1.20E+04
−6.25E+07.....	8700.	3.50E−06	3.50E−06	2.61E+06	3.77E+04	3.35E+04
−5.36E+07.....	8400.	1.70E−05	1.70E−05	1.32E+07	1.44E+05	1.23E+05
−4.47E+07.....	8000.	9.00E−05	9.00E−05	7.35E+07	6.16E+05	4.99E+05
−3.63E+07.....	7600.	4.70E−04	4.70E−04	4.04E+08	2.78E+06	2.14E+06
−2.93E+07.....	7300.	2.00E−03	2.00E−03	1.79E+09	9.67E+06	6.88E+06
−2.48E+07.....	7000.	5.20E−03	5.20E−03	4.87E+09	2.00E+07	1.27E+07
−1.89E+07.....	6000.	2.10E−02	2.10E−02	2.30E+10	4.93E+07	1.64E+07
−1.57E+07.....	3600.	5.90E−02	5.90E−02	1.08E+11	4.23E+07	1.57E+07
−1.44E+07.....	2800.	1.10E−01	1.10E−01	2.59E+11	1.38E+07	1.48E+06
−1.35E+07.....	2156.	2.00E−01	2.00E−01	6.16E+11	1.35E+07	1.43E+04
−1.28E+07.....	2187.	3.40E−01	3.40E−01	1.03E+12	1.80E+07	5.53E+01
−1.21E+07.....	2223.	5.60E−01	5.60E−01	1.68E+12	2.31E+07	1.34E−01
−1.13E+07.....	2264.	9.30E−01	9.30E−01	2.73E+12	3.02E+07	4.53E−03
−1.05E+07.....	2313.	1.60E+00	1.60E+00	4.61E+12	4.22E+07	7.18E−03
−9.74E+06.....	2367.	2.70E+00	2.70E+00	7.59E+12	6.07E+07	1.52E−02
−8.86E+06.....	2426.	4.80E+00	4.80E+00	1.32E+13	9.62E+07	4.18E−02
−7.94E+06.....	2482.	8.60E+00	8.60E+00	2.31E+13	1.62E+08	1.20E−01
−7.05E+06.....	2553.	1.50E+01	1.50E+01	3.91E+13	2.73E+08	4.48E−01
−6.07E+06.....	2627.	2.70E+01	2.70E+01	6.84E+13	4.88E+08	1.67E+00
−5.05E+06.....	2709.	4.90E+01	4.90E+01	1.20E+14	8.94E+08	6.91E+00
−4.02E+06.....	2799.	8.80E+01	8.80E+01	2.09E+14	1.60E+09	3.18E+01
−2.92E+06.....	2896.	1.60E+02	1.60E+02	3.67E+14	3.00E+09	1.58E+02
−1.93E+06.....	3003.	2.70E+02	2.70E+02	5.97E+14	5.47E+09	8.62E+02
−1.02E+06.....	3123.	4.30E+02	4.30E+02	9.12E+14	1.01E+10	5.20E+03
−1.70E+05.....	3240.	6.50E+02	6.50E+02	1.33E+15	1.83E+10	3.01E+04
1.88E+05.....	3310.	7.70E+02	7.70E+02	1.54E+15	2.47E+10	6.81E+04
5.50E+05.....	3398.	9.10E+02	9.10E+02	1.77E+15	3.50E+10	1.96E+05
7.59E+05.....	3478.	1.00E+03	1.00E+03	1.90E+15	4.54E+10	4.83E+05
1.18E+06.....	3622.	1.20E+03	1.20E+03	2.18E+15	7.39E+10	2.37E+06
1.37E+06.....	3765.	1.30E+03	1.30E+03	2.27E+15	1.05E+11	8.20E+06
1.55E+06.....	3878.	1.40E+03	1.40E+03	2.38E+15	1.36E+11	2.35E+07
1.90E+06.....	4118.	1.60E+03	1.60E+03	2.56E+15	2.09E+11	1.91E+08
2.06E+06.....	4243.	1.70E+03	1.70E+03	2.64E+15	2.46E+11	5.37E+08
2.53E+06.....	4594.	2.00E+03	2.00E+03	2.87E+15	3.44E+11	8.19E+09
2.82E+06.....	4912.	2.20E+03	2.20E+03	2.95E+15	4.42E+11	6.31E+10
3.24E+06.....	5256.	2.50E+03	2.50E+03	3.13E+15	7.81E+11	3.48E+11
3.51E+06.....	5688.	2.70E+03	2.70E+03	3.12E+15	1.97E+12	1.48E+12
3.66E+06.....	6321.	2.80E+03	2.80E+03	2.91E+15	7.35E+12	6.76E+12
3.81E+06.....	6825.	2.90E+03	2.90E+03	2.78E+15	1.88E+13	1.81E+13
3.96E+06.....	7245.	3.00E+03	3.00E+03	2.69E+15	3.75E+13	3.67E+13
4.12E+06.....	7799.	3.10E+03	3.10E+03	2.54E+15	8.22E+13	8.13E+13
4.30E+06.....	8143.	3.20E+03	3.20E+03	2.47E+15	1.27E+14	1.26E+14

bound-free edges of Ca I $4p\ ^3P^o_{2,1,0}$ at 2927.7 Å (level excitation energy of 1.879 eV), 2932.1 Å (1.886 eV), and 2941.3 Å (1.899 eV). Once again, the depth-independent PCS with the CRD length at 8 Doppler widths reproduces this line with $\xi = 3$ km s^{-1}. The comparison displayed in Figure 8 represents a calculation made with the same ξ and x_{CRD} for Mg I as assumed for the Mg II lines of Figure 6. We found it impossible to get the self-absorption part of the profile narrow enough with the large microturbulent velocity needed for the C II] lines. The synthetic profile is still broader than the observations, but this comparison suggests the Mg I emission also suffers from overlying absorption on both the red (~2853.0 Å) and blue (~2851.25 Å) sides of the profile. If these dips are truly due to overlying absorption, the λ2853.0 feature corresponds to the location of the Na I resonance lines at 2852.828 Å and 2853.031 Å. The λ2851.25 feature has no suitable neutral metal line that is coincident, assuming that the circumstellar environment is static with respect to the photosphere. The nearest reasonable candidate is Co I (UV2) at 2850.947 Å. Once again we remind the reader that the spectrum is noisy in this region and one should not place too much weight on these dips in the Mg I emission.

We also compared the observed semiforbidden Al II] line at 2669.2 Å to the synthetic profile. This line is also formed at the same depth at the C II], Mg I, and Mg II lines discussed above. The calculations with a constant microturbulent velocity of 3 km s^{-1} throughout the atmosphere once again produced a line much narrower than the observations. The increased ξ in the

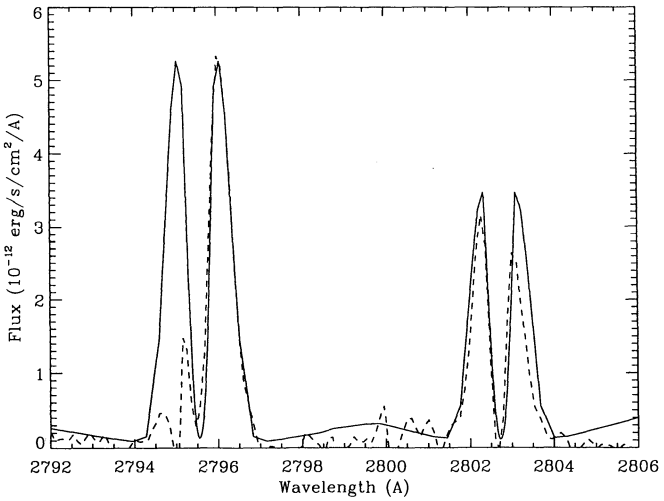

FIG. 6.—The Mg II *k* and *h* lines calculated for the final model (*solid*) compared with the *IUE* observations (*dashed*). The theoretical curve has been scaled to 18.0 mas and convolved with the *IUE* instrument profile. The calculations were performed under the assumption of depth-independent PCS with a CRD length of 3 Doppler widths and an enhanced microturbulent velocity at the depth of formation of these emission features.

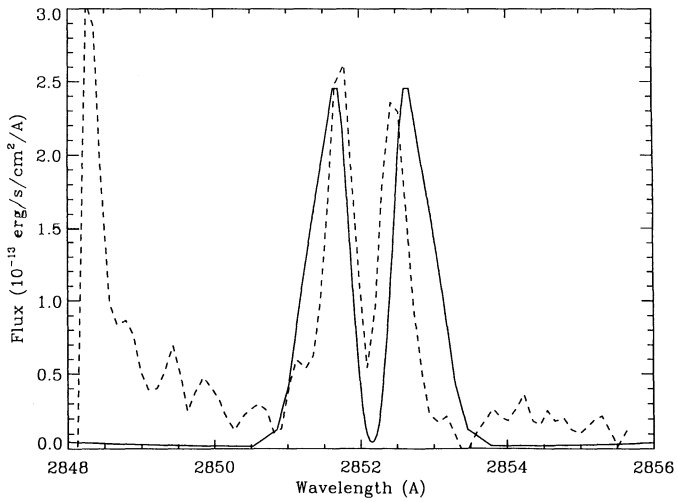

FIG. 8.—The calculated Mg I λ2852 line profile (*solid*) compared with the *IUE* observations (*dashed*). For this comparison, the model is scaled to an angular diameter of 20.0 mas and convolved with a Gaussian of 0.18 Å. The depth-independent PCS approximation is used for the redistribution function with the CRD length at 3 Doppler widths. The same microturbulent velocity is used here as in Fig. 6.

lower chromosphere used for the profiles in Figures 6–8 reproduce this feature more closely, as was the case for the C II] intersystem lines. This line, like the C II] lines, had to be scaled such that the model has an angular diameter of 4.1 mas (i.e., it is too bright in the model). In these comparisons, we have ignored absorption by interstellar dust, whose opacity peaks near 2200 Å. Should interstellar reddening be significant for this star, it would help contribute to the flux differences seen between the Al II] and C II] synthetic lines and the observed spectrum. Finally, these results may indicate that the abundance of aluminum in g Her may be lower than in the Sun.

We now make comparisons of the synthetic spectra of this model to ground-based observations made with the McMath telescope. Since the McMath stellar CCD has a great enough dynamic range to record both the line core and the photospheric line wings, and the star is brighter in the visual and near-infrared than in the ultraviolet, bound-bound opacities from other metals can clearly be seen in the wings of the strong resonance transitions in these spectral regions. The technique used to include "supplemental" bound-bound opacities into PANDORA has been described by Avrett et al. (1986). The scattering albedo α, as described by these authors, has been modified so that it is determined analytically by

$$\alpha = \frac{1}{1+x}, \tag{7}$$

where x is a function of wavelength λ (in angstroms) and electron density n_e (in cm^{-3}) as described by Anderson (1989):

$$x = \frac{n_e}{1.07 \times 10^{14}} \left(\frac{\lambda}{5000}\right)^3 . \tag{8}$$

Since our model typically has electron densities less than 10^{14} cm^{-3}, α is near unity throughout most of the model (i.e., photons are nearly all scattered in the lines, few are absorbed). Note that the opacity "look-up" table has rather a coarse wavelength grid, so detailed high-resolution comparisons are not possible. The background-line opacity for the wavelength points in the NLTE line profiles are interpolated from the two closest opacity reference wavelengths in the look-up table. Figure 9 shows a comparison between the Ca I synthetic resonance line at λ4227 to the observations. Since the uncertainty in the absolute flux calibration of the ground-based observations range between 10% and 25%, we do not scale the model to a given angular diameter but scale the flux to achieve the best fit. From the comparison in Figure 9, the red side of the Ca I line wing ($\Delta\lambda > 5$ Å) fits rather well to the observed flux. Since $S_\nu = B_\nu$ at the formation depths ($m > 88$ g cm^{-2}) for these wavelengths and the CRD fluxes match the PRD fluxes in this region of the profile, we claim that the photospheric portion of our model is somewhat representative of g Her. Note that the

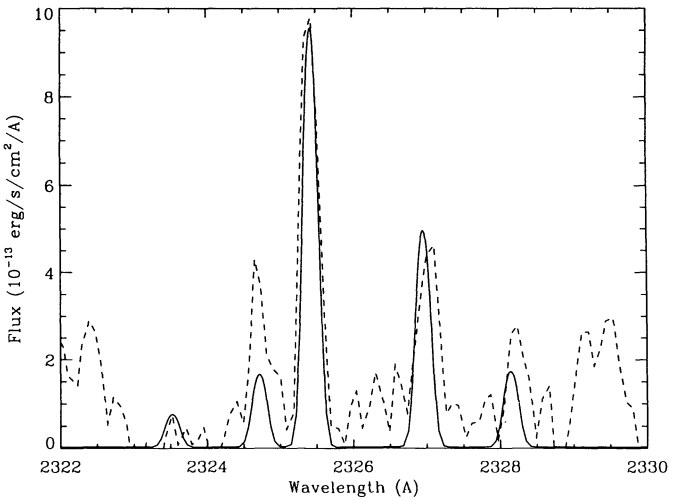

FIG. 7.—The C II] UV0.01 multiplet as calculated for the final model T10 (*solid*) is compared with the *IUE* observations (*dashed*). The synthetic flux is scaled to 7.0 mas and convolved with a Gaussian of 0.13 Å. The synthetic profiles presented here are calculated with an enhanced microturbulence velocity as described in the text.

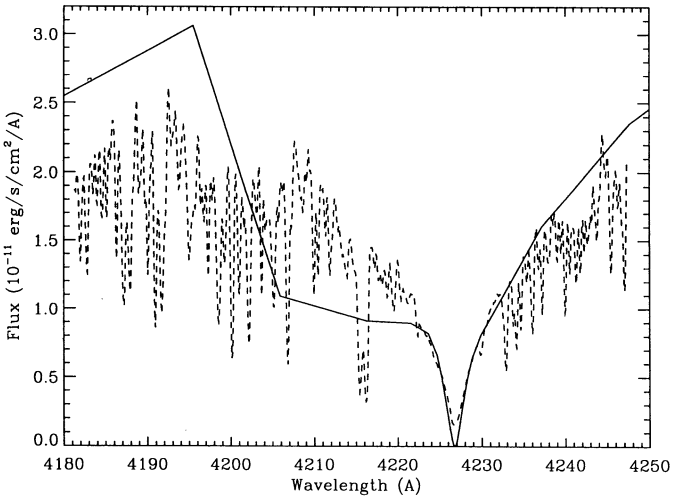

FIG. 9.—The Ca I λ4227 profile of the final model T10 (*solid*) compared with the McMath observations. For this comparison, the synthetic flux is scaled to achieve the best fit (see text) to the observations and convolved with an instrument profile of 0.20 Å. The "strange" shape to the wings of the line profile is due to the inclusion of supplemental bound-bound opacities from the Kurucz opacity look-up tables and the coarseness in frequency-space of this look-up table.

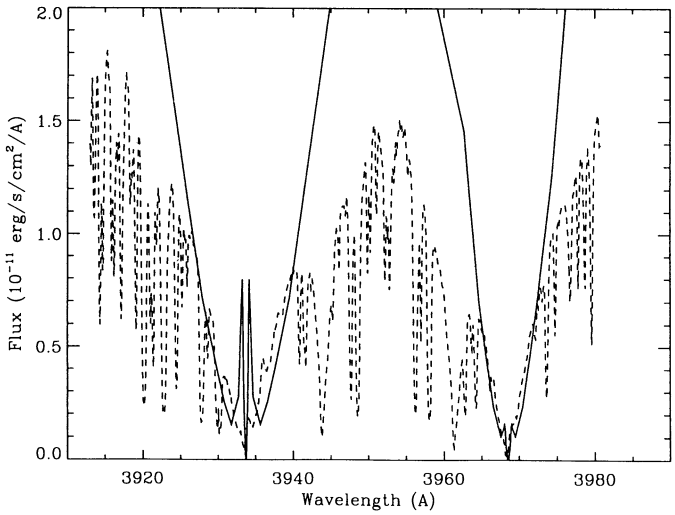

FIG. 10.—The Ca II H and K profiles of the final model (*solid*) compared with the McMath observations (*dashed*). The profiles were calculated with the depth-dependent PCS approximation, the flux scaled to achieve the best fit, and convolved with a 0.11 Å FWHM Gaussian which is representative of the McMath's instrument profile for this observation. We display the profiles without the inclusion of the Kurucz background bound-bound opacities in the emergent flux calculation to show the effect line blanketing has on the line wings and continuum in this region of the spectrum.

core of the line is formed in the lower chromosphere but does not display any chromospheric emission due to the collisional rates being too small compared to the photoionization rates for this transition.

We next compare the synthetic profiles of Ca II to the ground-based McMath observations. The "chromospheric" emission features of H and K, which are very prominent in warmer M giants, are very weak in g Her and take on more of the appearance of a "plateau" instead of "emission bumps." We first assumed a depth-dependent x_{CRD} for PCS as done initially for Mg II. For the test runs with $\xi = 3$ km s^{-1} at all depths, substantial emission resulted in the core of the Ca II H and K lines (see Table 2), and the Ca II IRT lines were much narrower than the observations. The level of formation for the peak flux in the Ca II resonance lines is just below the depth at which Mg II *h* and *k* form ($m = 5.9 \times 10^{-2}$ g cm^{-2}), while the infrared triplet cores ($\Delta\lambda = 0.2$ Å) form throughout the lower chromosphere from $2.0 \times 10^{-3} \leq m \leq 5.9 \times 10^{-2}$ g cm^{-2}. The narrow Ca II IRT features are consistent with the deviations between the synthetic spectra and the C II] and Al II] observations, which again suggests the microturbulent velocity is enhanced in the lower chromosphere to values greater than the sound speed. We next calculated these line profiles for model T10 with the enhanced microturbulent velocity in the lower chromosphere. These calculations produced broader Ca II IRT lines which more closely reproduce the observations. The increased microturbulent velocity at the H and K "core" depths, leads to weaker, broader emission due to core photons being able to migrate farther out into the wings and due to a broadening of the central self-reversal. Figures 10 and 11 show these Ca II H and K and the Ca II infrared triplet (IRT) synthetic profiles in comparison with the McMath observations, respectively. The Ca II H line has essentially no emission peak compared to the K line; the H line emission takes on the appearance of a "plateau" like the observations. This results from the factor of 2 difference between the opacity of these two effectively thin lines—these lines are formed in the steep temperature gradient regime of the lower chromosphere and the contribution function of the H line samples a larger percentage of lower temperature depths than the K line. The K line synthetic profile has significant emission which is not seen in the observations. Could this emission be obscured by circumstellar absorption? A strong Ti I line resides at 3934.228 Å which could account for a depressed flux on the red side of the Ca II K line core. No significant neutral metal lines reside on the blue side; however, the self-reversal is shifted slightly blueward from

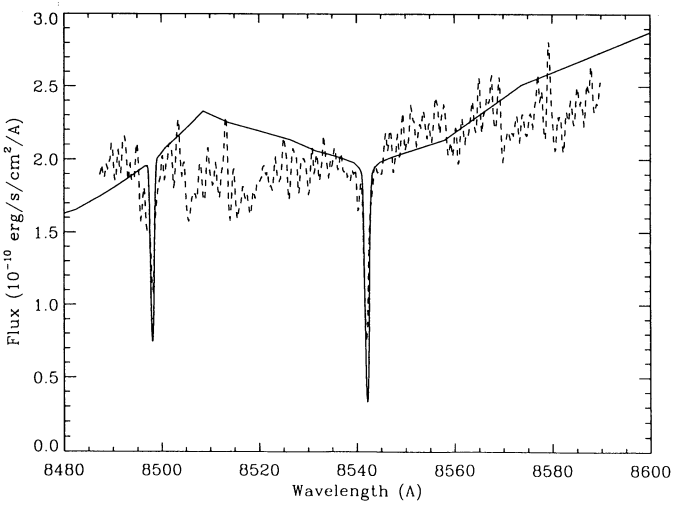

FIG. 11.—Two of the Ca II infrared triplet synthetic profiles (*solid*) compared with the McMath observations (*dashed*). The synthetic flux is calculated with the inclusion of the background Kurucz line opacities and is scaled to achieve the best fit with the observations and convolved with a 0.51 Å FWHM Gaussian. Although the cores of these lines are formed in the lower chromosphere, they are pure absorption features and compare well with the observations. The microturbulent velocity profile of Fig. 6 is used here and is required to match the width of the observed lines.

the onset of the stellar wind and *may* obliterate much of the emission on this side of the line. We note here that the T5 chromosphere has a weaker K emission feature than the T10 model due to a slightly lower temperature at its formation depth. Model T5 however produces a slightly weaker Hα feature as compared to T10, which does not match the observations as well (see below).

Finally we model the Hα line of g Her and display it in Figure 12 along with the McMath observation of this spectral region. This observation also includes the strong Ca I line at 6573 Å. This Ca I line is formed solely in the photosphere (line center depth of formation at 0.56 g cm^{-2}) and the ratio of the depth of this absorption line to the depth of the Hα line can be used as a measure of the validity of the chromospheric model (see Table 2). The Hα line core is formed at 2.1×10^{-2} g cm^{-2} at $\mu = 1$ and 5.2×10^{-3} g cm^{-2} at $\mu = 0.3$—the depth of formation of most of the Mg II *h* and *k* emission. We should point out here that for hydrogen calculations in a "pure" photospheric model with an effective temperature and surface gravity representative of g Her, the Hα profile is so weak that it would not be seen among the strong TiO lines in the region (see Luttermoser & Johnson 1992). The fact that we see this line in the spectrum of g Her indicates that it is chromospheric in nature. Also mentioned by Luttermoser & Johnson (1992) was the fact that PRD in the Lyα line has a significant impact of the strength of the Hα line for this model. Partial redistribution in Lyα enhances the number density of the first excited state over CRD calculations in the lower chromosphere, enough for the Hα line to form there. We note here that the T10 model (with Lyα in PRD) ratio of the line center fluxes between Ca I and Hα, F_o(Ca I)/F_o(Hα), is ~0.72, whereas the observations give 1.12. This may suggest that the chromosphere should be hotter at the depth of formation of this feature. This would influence the other chromospheric indicators greatly and make the fits worse. A more likely explanation to the discrepancy between the Hα line and the Ca I λ6573 line is the PCS assumption used the PRD calculations of Lyα. An exact calculation of the R_{II} redistribution function (e.g., see Gayley 1992) may give rise to a closer fit between these two absorption lines in our model.

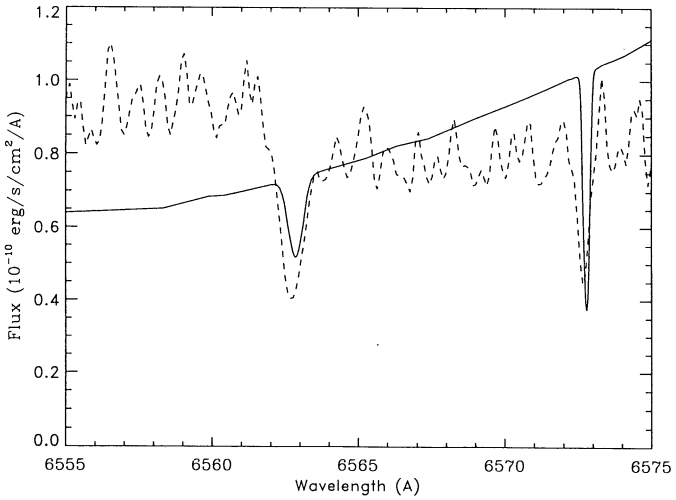

FIG. 12.—A comparison between the NLTE synthetic profiles of Hα and Ca I λ6573 (*solid*) and the observed spectrum of g Her (*dashed*) in this region. Note that the coarse grid of background bound-bound opacities from various atomic and molecular species have been included in the flux calculations. The Ca I feature is purely photospheric while the Hα feature is formed in the chromosphere. The ratio of the line center fluxes of these lines hence indicates chromospheric activity in this star.

4. DISCUSSION

Because of discrepancies among the results for C II], Mg II, and Hα, we have been unable to fit even the best available chromospheric diagnostics with a single plane-parallel, hydrostatic, homogeneous *classical* chromospheric model. These discrepancies had the following form: In order to get the electron density high enough with a traditional model, the lines must form at such high mass column density that Hα becomes much too strong, some photospheric lines develop unobserved emission cores, and the wings of Mg II *h* and *k* become much too broad. Other discrepancies include the ratios of emission lines. While C II], Al II], Mg II, and Mg I are formed in roughly the same part of the chromosphere, the emission portion of the Mg I and Mg II features form over a range from $4.7 \times 10^{-4} \leq m \leq 5.9 \times 10^{-2}$ g cm^{-2} and $3.5 \times 10^{-6} \leq m \leq 27$ g cm^{-2}, respectively. Indeed, the peak flux of the Mg I and Mg II line originate from the same depth ($m = 2.1 \times 10^{-2}$ g cm^{-2}) as the formation depths of the C II] and Al II] emission lines and the core of Hα. This coincidence arises quite naturally in this one-dimensional, hydrostatic modeling, for we need to find a temperature rise to produce both Mg II and Mg I emission. If we raise the temperature too far out, the density is too low for Mg I to have sufficient opacity for emission features to form at the typical chromospheric temperatures (i.e., 5000–7000 K), whereas Mg II still possesses sufficient opacity, due to its slightly higher number density at these temperatures as compared to Mg I, to produce emission. We cannot start the temperature rise too deep since observed "photospheric" absorption lines (i.e., Mg I λ4571) go into emission. Due to these constraints, the temperature rise must begin around $m = 0.1$–0.3 g cm^{-2} and increase dramatically to temperatures between 5000 and 7000 K at around 0.02 g cm^{-2}. Such a sharp temperature rise suggests that a shock structure may exist in this region of the atmosphere.

4.1. *Electron Densities*

The observed C II] line ratios indicate the electron density should be increased in our model by an order of magnitude. The hydrogen density is quite low at the formation depth of these lines, and one would have to increase the temperature at this depth to well over 10,000 K to produce the observed ratios. This, of course, would produce enormous Balmer emission lines (as seen in Mira variable stars) which have not been seen in this star. This discrepancy can also be remedied by moving the chromosphere in to lower depths, but then one runs into the problems mentioned above. There is the possibility that the C II] ratios are unrepresentative of this star because of noise in the *IUE* spectra near 2325 Å (GHRS observations of these very cool giants would be invaluable), but the appearance of this multiplet here is very similar to that in the M5 III star 2 Cen (Eaton & Johnson 1988), the only other M giant this cool observed in the C II] lines. At the formation depth of the C II] lines and the peak flux of the Mg II lines, H I contributes 64.0% of the electrons followed by O I (20.6%), C I (8.5%), Ne I (1.1%), and N I (1.0%). Both hydrogen and carbon are handled in NLTE, while the rest are in LTE. Carbon is 96.8% ionized at this depth and $n_\kappa/n_\kappa^* \approx 1$, indicating that we cannot increase the electron density at these depths with

carbon. Hydrogen is 64% ionized at this region and is severely underionized with respect to LTE (~3 orders of magnitude). Luttermoser & Johnson (1992) have shown that the Lyman lines act as a *drain* in the chromosphere of late-type giants and that PRD gives the same level/ion densities as CRD at these depths. Hence, we cannot enhance the electron density at this region of the atmosphere from a better treatment of hydrogen (i.e., including more levels will slightly enhance the Lyman-line drain). One might expect oxygen to have similar ionization properties as hydrogen, since it has nearly the same ionization potential and has strong UV resonance lines. Radiative transfer in the oxygen atom is very complicated however. Field & Steigman (1971) have shown that the charge-exchange reaction rate $O + H^+ \Leftrightarrow O^+ + H$ can dominate the ionization equilibrium of oxygen in low-density environments. This charge-exchange reaction for our model in the Mg II emission region would give $n(O^+)/n(O) \approx 9/8 n(H^+)/n(H)$—oxygen underionized with respect to LTE which would substantially reduce the electron density. Haisch et al. (1977), however, have shown the importance of the Lyβ-pumped fluorescence mechanism to the excitation of the 1302–1306 Å resonance lines of the O I atom. The $^3P_2$–^3D excitation at 1025.77 Å via Lyβ photons, followed by an immediate ionization out of the ^3D state from the intense far-IR photospheric radiation field of this star, might give rise to an overionization of O I with respect to LTE. Such a mechanism could enhance the electron density in the lower chromosphere and rectify the C II] line ratio problem; however, Carlsson & Judge (1993) have determined that this scenario will not work. Unfortunately, we cannot further test this mechanism since such a calculation involving fluorescence is currently not possible with PANDORA. The likely explanation to the electron density discrepancy probably involves our omission of hydrodynamic processes, which will enhance the gas density at these depths, and possible inhomogeneities in the atmospheric structure (see Ayres 1990; Jørgensen & Johnson 1991; and Wiedemann & Ayres 1991). Finally, an increase in the surface gravity by an order of magnitude would help to rectify this problem.

4.2. Ca II H and K

The chromospheric emission features in the Ca II H and K line cores of g Her (and most cool giant stars) are observed to be too weak relative to Mg II *h* and *k*. From this study, we can identify several reasons for this inconsistency. (1) The thermalization of photons scattering in the line wings is dominated by collisional de-excitation (i.e., depth-dependent PCS) instead of continuum processes (i.e., depth-independent PCS) as was the case for the Mg II lines. This results in the Ca II chromospheric emission flux being weaker and broader than would be the case for depth-independent PCS. (2) The enhanced mircoturbulent velocity in the lower chromosphere further broadens the Ca II emission, depressing the peak flux further. (3) Boesgaard & Hagen (1979) have also suggested that the weakness could further be the result of increased attenuation in a wind that absorbs over the entire range of velocity of the Ca II emission features. We do not place too much weight on this suggestion, since it is difficult to understand why a large velocity gradient presents itself in the formation region of the Ca II cores (i.e., the H_3 and K_3 features) and is not evident in the Mg II line cores which are formed slightly higher in the atmosphere. Instead, we simply claim that the chromospheric velocity field shifts the K_3 and H_3 features slightly blueward to help hide some of the chromospheric emission. (4) We also need to rely on overlying absorption from netural metals to explain the weakness of the features.

4.3. *Inhomogenieties or Hydrodynamic Shocks?*

Based upon the inconsistencies between the synthetic and observed spectra for g Her, we have developed two scenarios: (1) geometric inhomogeneities in the chromosphere; and (2) hydrodynamic processes giving rise to shock structures within the atmosphere. To test the inhomogeneity question, we have taken model T10 to represent our best model to fit the strong resonance lines with the observations and model T7 to represent our best model for the optically thin transitions. For our argument here, we assume that g Her has an angular diameter of 28.0 mas (based upon the low-dispersion *IUE* spectrum), and we ignore ISM absorption and limb darkening (or brightening). To fit the Mg II *h* and *k* lines in model T10, an angular diameter of 17.5 mas was required. This gives a filling factor 0.63 for the Mg II emission region. To fit the C II] lines from model T7, an angular diameter of 0.35 mas was needed, giving a filling factor of 0.013. In both models, much of the Mg II emission comes from the same depth as the C II] emission. Scaling in the filling factors with the integrated fluxes of Table 2, 83% of the C II] comes from an area of the stellar disk with a temperature structure similar to T7, while 17% comes from an area similar to the temperature structure of T10. As a result, the emergent flux would be dominated by the T7 model region (i.e., no inconsistencies). Meanwhile, 86% of the Mg II flux comes from the T7 model region and 14% from the T10 model region. Once again the emergent flux from the T7 model region would dominate which leads us to an inconsistency, since the emergent Mg II lines look like the T10 model, not the T7 model. As a result, large-scale inhomogeneities in the chromospheric structure *cannot* be invoked to explain the inconsistencies between the Mg II profiles and the C II] line flux ratios.

Since inhomogeneities do not seem to be the answer, the assumption of hydrostatic equilibrium in these late-type atmospheres must be examined—do dynamical processes dominate the atmospheric structure? Subjecting chromospheric models to the equation of continuity with inferred values of mass loss and observed values of outflow velocity leads to the conclusion that some agent is needed to puff out the chromosphere in carbon stars (Johnson 1991). Recent dynamic models of late-type pulsating giant stars (i.e., Miras) have shown that long-period waves set up by the pulsations turn into shocks as the waves propagate down the density gradient of the atmosphere (Bowen 1988; Fleischer, Gauger, & Sedlmayr 1992). These shocks greatly extend the atmosphere and enhance the gas density many orders of magnitude above the hydrostatic equilibrium result. Bowen has shown that a typical nondusty models produces a region of enhanced temperature, extending typically from 2 to 5 R_*, which persists throughout the pulsational cycle and resembles a typical static chromosphere. Luttermoser et al. (1993) have shown that the existence of these hydrodynamic chromospheres in shocked atmospheres give rise to the peculiar maximum light phase shift (0.3–0.5) between the hydrogen Balmer lines and the Mg II *h* and *k* lines seen in Miras. Perhaps such a *shocked* chromosphere could help explain the discrepancy between the Mg II and C II] lines. The semiregular variable g Her is not a Mira star, however, and Balmer emission lines have not been seen. If g Her is weakly pulsating and these pulsations give rise to multiple shocks in the atmosphere, the shocks must never get above

$\sim$5000 K in temperature and must not appear until the acoustic waves reach a column mass of less than ~ 1 g cm^{-2} in order to keep the Mg I and Mg II flux ratios close to the observed values and prevent the Balmer lines from becoming emission features. We do not attempt to carry out hydrodynamic calculations or to carry out radiative transfer calculations based upon such models in this paper. Such work is now being undertaken.

4.4. *Circumstellar Environment*

Late-type giant stars earlier than M5 show substantial winds in the Mg II and Ca II resonance line profiles (see Boesgaard & Hagen 1979; Stencel & Mullan 1980; Eaton & Johnson 1988). This star is known to be losing mass at a rate of $\sim 2 \times 10^{-7}$ $M_\odot$ yr^{-1} from the CO $J = 2$–1 transition (Wannier & Sahai 1986). Also, giant stars with spectral types M5 and later typically display severe overlying absorption from neutral metals in the profiles of these lines (Eriksson et al. 1986; Eaton & Johnson 1988) which makes it difficult to detect the wind absorption component of the line. Indeed, Luttermoser et al. (1989) *assumed* that the emission wing on the shortward side of the Mg II *h* line was uncorrupted by such overlying absorption in order to deduce the chromospheric model and velocity profile of the gas for TX Psc. The profiles of g Her also show this overlying absorption. The high-resolution spectra of the *optically thin* C II] profiles are uncorrupted by overlying absorption, and we can use these lines to deduce the macroscopic velocity field. As was found by Luttermoser et al. (1989) in the chromospheric model of TX Psc, the C II] lines are formed in roughly the same atmospheric region as the emission features of the Mg II lines in the final model. The C II] lines in g Her are found at the same radial velocity as the photospheric lines (i.e., 3 km s^{-1}), which indicates that no appreciable macroscopic flows exist in the lower chromosphere for the model (in contrast to the situation deduced for TX Psc). These C II] lines, unfortunately, tell us nothing about the flow farther out; however, the Mg II and Ca II line cores *suggest* a slight wind component may exist. By examining the depth of formation of these "wind" features, we see that the stellar wind must commence near a column mass of 10^{-6} g cm^{-2}— $\sim 5 \times 10^7$ km (0.1 R_*) above the depth of formation of the peak of the Mg II emission (i.e., 7×10^7 km, or 0.16 R_*, above the continuum formation depth at 5000 Å) with a velocity of approximately 10 km s^{-1}. We also take the obscuration of circumstellar lines of Mn I, Fe I, and other neutral elements into effect by convolving a Gaussian profile for these lines into the Mg II profiles. We calculated the attenuation by these features with a slab-model approximation for an assumed cool circumstellar shell (CS) that lies at least 0.2 R_* above the photosphere (i.e., above the depth of formation of the Mg II emission features). Table 5 identifies the CS lines used in this calculation. The emergent flux of this slab model is simply calculated from the attenuation of the chromospheric flux in the slab via

$$F_{cs} = F_* e^{-\tau_{cs}}, \tag{9}$$

where

$$\tau_{cs} = 8.85 \times 10^{-21} N_i f_{ij} \phi_{ij} \lambda_o^2, \tag{10}$$

$$N_i = \alpha \frac{N_H}{0.908} \frac{g_i}{g_o} e^{-E_i/kT_{ex}}, \tag{11}$$

$$\phi_{ij} = e^{-(\lambda - \lambda_o)^2/\delta_{cs}^2}/1.77\delta_{cs}, \tag{12}$$

TABLE 5

CIRCUMSTELLAR ABSORPTION LINES

Line ID	λ_{air} (Å)	log $g_i f_{ij}$	E_i (eV)
Fe I	2793.865	−1.0	2.50
Fe I (UV46)	2794.700	−2.4	0.95
Mn I (UV1)	2794.817	+0.5	0.00
Fe I (UV3)	2795.006	−2.2	0.00
Fe I (UV44)	2795.540	−1.7	0.91
Cr I	2795.703	−2.1	2.54
Cr I	2795.919	−1.5	2.54
Cr I	2795.939	−2.4	2.51
Mn I (UV1)	2801.084	+0.5	0.00
Fe I (UV3)	2803.169	−3.2	0.05
Fe I (UV44)	2804.521	−0.6	0.91

and f_{ij} is the oscillator strength of the transition, which were taken from Kurucz & Petrymann (1975); λ_o is the central wavelength of the transition in angstroms, Doppler-shifted to the radial velocity of the shell with respect to the photosphere; α is the abundance of the element; N_H is the hydrogen column density of the shell (hydrogen abundance is assumed to be solar—0.908); g is the statistical weight ("o" denotes ground state), where we assume the partition function $U = g_o$; E_i is the energy level of the lower state of the transition; T_{ex} is the excitation temperature of the ith state; finally $\delta_{cs} = \lambda_o(\langle v_{cs} \rangle/c)$, where $\langle v_{cs} \rangle$ is the velocity dispersion of the Gaussian profile. The CS lines are calculated under the assumption solar abundance (Anders & Grevesse 1989). Initially, we needed a hydrogen column density of 1.5×10^{22} cm^{-2} in order to get a reasonable fit on the shortward side of the *k* line and to see at least some absorption on the longward side of the *h* line from overlying absorption. For this large of a value, the CS shell would extend into the lower chromosphere of our classical models ($m \sim 2 \times 10^{-2}$ g cm^{-2}), near the formation depth of the Mg II emission. However, this value is similar to the circumstellar column density overlying the Mg II lines in N-type carbon star TX Psc as deduced by Eriksson et al. (1986).

We next checked the effect of various input parameters used in the CS attenuation. We scaled the abundance of Fe I from the solar value of 3.89×10^{-5} to 7.59×10^{-5}, which represents the upper limit of the uncertainty of the iron abundance in g Her deduced by Smith & Lambert (1985). This had a slight impact on the appearance of the CS features. It has been suggested by Phillips (1979) that the oscillator strengths calculated by Kurucz & Petrymann (1975) for intercombination lines may well be several orders of magnitude too small. As a result, we increased the oscillator strength of the Fe I UV3 transitions by a factor of 10 with respect to the Kurucz & Petrymann values; these new values are tabulated in Table 5. Figure 13 represents the results of these modifications. The CS absorption in this figure has a hydrogen column density of 3×10^{20} cm^{-2}. The overlying lines are relatively insensitive to the excitation temperature, from an assumed shell temperature of 1000 K to the radiation temperature of the Mg II emission of 3200 K. We needed a rather large velocity dispersion of 18 km s^{-1} for the CS lines, infalling at 5 km s^{-1} with respect to the frame of the stellar photosphere. The CS absorption that overlies the longward side of the Mg II *h* line is not reproduced as well as the shortward side of the *k* line. This may suggest that the oscillator strength of the Fe I line at 2803.2 Å is larger than the value quoted in Table 5.

Our final column density of 3×10^{20} cm^{-2} extends into our classical model chromosphere T10 as well, but lies 1×10^7 km

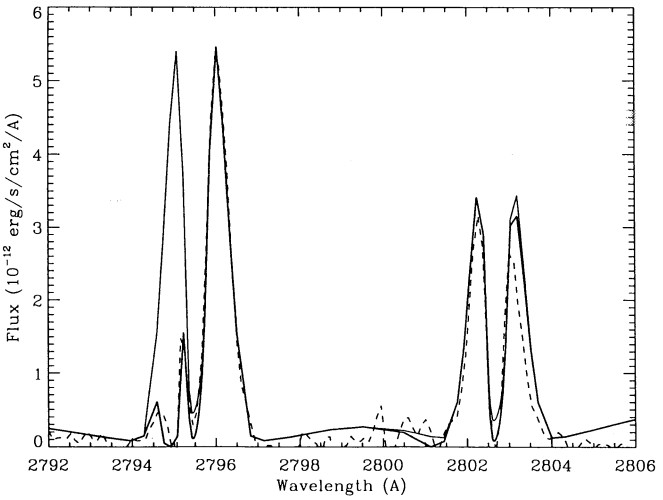

FIG. 13.—The Mg II k and h lines including the effects of a macroscopic velocity field are displayed along with the *IUE* observations (*dashed*). A comparison is also made between the emergent fluxes of these synthetic lines with no CS absorption (*thin solid*) to that with absorption of a CS shell of hydrogen column density 4×10^{23} cm^{-2} (*thick solid*). Note that the flux has been scaled to an angular diameter of 17.5 mas to achieve the best fit.

($\sim 0.03\ R_*$) above the Mg II emission region. We remind the reader that this CS modeling is crude at best, since it ignores sphericity, possible inhomogeneities in the CS shell, scattering and other NLTE effects.

Tsuji (1988) has made high-resolution infrared spectra of the low-excitation lines of the CO first overtone band for g Her, and deduced log $N_{CO} = 19.49$, $T_{ex} = 1212 \pm 128$ K, $v_{rad} = -2.0$ km s^{-1} (i.e., infall), and $\xi > 3$ km s^{-1}. For an assumed temperature of 1000 K, the velocity dispersion used for our CS Gaussian profiles indicates that width of the CS lines is almost entirely due to microturbulence. The small infall velocity of 5 km s^{-1} we deduced is consistent with the CO observations of Tsuji (1988). We note here that we were also able to obtain a good fit to the observed Mg II lines with linear (with respect to height) macroscopic gas velocity profile, scaling from 5 km s^{-1} at 0.2 g cm^{-2} to 50 km s^{-1} at 6.5×10^{-15} g cm^{-2}. We however chose the velocity profile in Figure 14 (which is still consistent with the Mg II observations) to reflect the near-static

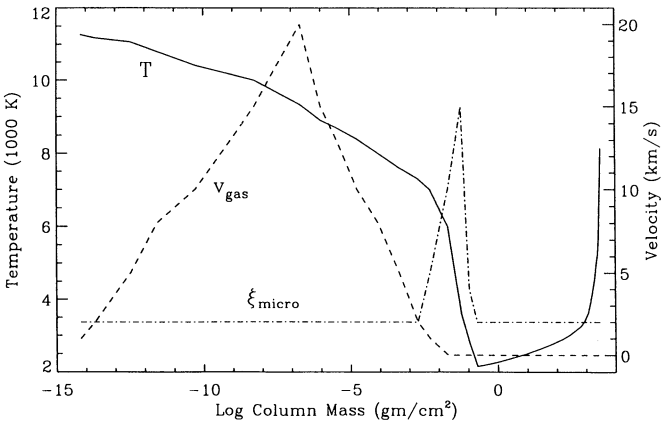

FIG. 14.—The temperature structure of model T10 (*solid*), the macroscopic (i.e., wind) velocity profile (*dashed*), and the microturbulent velocity profile (*dot-dashed*) are displayed as a function of column mass. This plot corresponds to the state of the model for the calculations displayed in Fig. 13.

condition of our CS shell. Tsuji attributes the formation depth of these lines to a quasi-static, turbulent transition zone between the chromosphere and stellar wind. With the carbon abundance of Smith & Lambert (1985), and if all the carbon is in the form of CO, the hydrogen column density from Tsuji's measurements is log $N_H = 23.1$. Our value of 20.3 is much lower than Tsuji's value and may suggest that there are large regions on the stellar disk that are cool at depths similar to the depth of formation of the Mg II emission (once again, an inhomogeneous chromosphere).

To achieve a better fit in the absorption cores of the Mg II lines (i.e., the k_3 and h_3 features), we included an interstellar component to the overlying absorption moving toward us at 7 km s^{-1} with a velocity dispersion of 3 km s^{-1}. We used a Mg II ISM column density of 2.6×10^{16} cm^{-2}. Using the empirical relation of Bohlin, Savage, & Drake (1978), this corresponds to reddening of $E(B-V) = 0.13$ assuming that most of the interstellar magnesium is in the singly ionized state and at solar abundance. The uncertainty of these ISM parameters are rather high, since the chromospheric model at the formation depth of the k_3 and h_3 features is uncertain, the observed spectrum is very noisy in these features, and our technique for subtracting off the ISM (and CS) absorption is crude. The column density can range anywhere between 1 and 6×10^{16} cm^{-2} and still give a reasonable fit with our technique.

5. CONCLUSIONS

Luttermoser & Johnson (1992) have already described the difficulties in carrying out NLTE calculations in cool, low-density, stellar atmospheres and the techniques one must use to converge a solution using the equivalent two-level approach. Since one must attempt to fit as many *chromospheric indicators* as one can access, many runs must be made for each atom and ion handled in NLTE. We have obtained a large number of observational constraints for g Her to carry out this analysis and have found that semiempirical techniques involving "classical" models under the assumptions of one-dimensional, homogeneous geometries in hydrostatic equilibrium cannot reproduce all of the spectral features of this star. We note here that we have begun to carry out preliminary calculations of a g Her model with similar characteristics to hydrodynamic models of Mira variables (i.e., a model with a permanent chromosphere, or "calorisphere," and outward propagating shocks, see Bowen 1988). We will show in a subsequent paper that many of the "chromospheric" spectral features of this semiregular variable can be reproduced with such a model.

This suggests that future modeling of these late-type variable stars, both the Miras and semiregulars, require atmospheric modeling with dynamic processes (see Bowen 1988) and possibly inhomogeneous geometries (see Jørgensen & Johnson 1991) included in the calculations. Previous semiempirical chromospheric models of late-type giants, based on a limited set of spectral features (e.g., the model for TX Psc by Luttermoser et al. 1989), are not true representations of the thermal structure of these stellar atmospheres.

This investigation leads to the following conclusions. (1) The chromospheric structure of semiregular, late-type giant stars (g Her as the prototype) cannot be described by the classical, one-component model in hydrostatic equilibrium. (2) Inconsistencies between ultraviolet emission features and infrared CO absorption suggest the outer atmosphere of these stars are inhomogeneous. (3) Such inhomogeneities, however, cannot

account for the difficulty in fitting both the C II] intersystem line ratios and the Mg II profiles—we suggest that hydrodynamic processes (i.e., shocks) may help resolve this problem. (4) Thermalization in the Mg II *h* and *k* lines in cool giant stars is controlled by continuum absorption and *not* collisional deexcitation as is the case for warmer K giants. (5) The chromospheric emission features (i.e., UV emission features) seen in these stars are formed relatively close to the star ($r \lesssim 0.05R_*$). (6) The circumstellar environment includes a cool component that resides above the chromosphere, which is relatively static and very turbulent with a hydrogen column mass of $\sim 3 \times 10^{20}$ cm^{-2}.

We thank Mr. Dave Jaksha of the National Solar Observatory for showing us how to use the McMath solar telescope and stellar spectrograph and for help with the preliminary data reductions of our ground-based observations. We thank Dr. Frederick Walter for help in reading FITS-formatted tapes, and Drs. Eugene Avrett and Rudolf Loeser for encouraging us to use their PANDORA stellar atmospheres code. Thanks are also extended to Dr. Philip Judge for helpful discussions and useful comments on the manuscript, and to an anonymous referee for additional comments. Finally, we wish to thank Drs. Sallie Baliunas, Louis Boyd, Russell Genet, and Greg Henry for the photometric results of g Her, which were obtained with the Smithsonian 0.25 m APT, operated jointly by the Smithsonian Astrophysical Observatory, Fairborn Observatory, and Tennessee State University and generously supported by SAO Director Dr. Irwin Shapiro. Use of the Colorado IUE-RDAF, supported by NASA contract NAG 5-28731, is acknowledged. This research was partially supported by NASA grants NAG 5-1181 and NAG 5-1777 to Iowa State University; NAG 5-1305 to the University of Colorado; NAG 5-182 to Indiana University; and NAG 5-1327 to Tennessee State University.

REFERENCES

Anders, E., & Grevesse, N. 1989, Geochim. Cosmochim. Acta, 53, 197
Anderson, L. S. 1989, ApJ, 339, 558
Avrett, E. H., & Loeser, R. 1984, in Methods in Radiative Transfer, ed. W. Kalkofen (Cambridge: Cambridge Univ. Press), 341
———. 1992, in Seventh Cambridge Workshop on Cool Stars, Stellar Systems, and the Sun, ed. M. S. Giampapa & J. A. Bookbinder (ASP Conf. Ser., 26), 489
Avrett, E. H., Machado, M. E., & Loeser, R. 1986, in The Lower Atmosphere in Solar Flares, ed. D. F. Neidig (Sunspot, NM: National Solar Observatory), 216
Ayres, T. R. 1990, in Sixth Cambridge Workshop on Cool Stars, Stellar Systems, and the Sun, ed. G. Wallerstein (ASP Conf. Ser., 9), 106
Ayres, T. R., Judge, P., Jordan, C., Brown, A., & Lnsky, J. L. 1986, ApJ, 311, 947
Basri, G. S., Linsky, J. L., & Eriksson, K. 1981, ApJ, 251, 162
Boesgaard, A. M., & Hagen, W. 1979, ApJ, 231, 128
Bohlin, R. C., Savage, B. D., & Drake, J. F. 1978, ApJ, 224, 132
Bowen, G. H. 1988, ApJ, 339, 299
Brown, A., & Carpenter, K. G. 1984, ApJ, 287, L43
Brown, J. A., Johnson, H. R., Alexander, D. R., Cutright, L., & Sharp, C. M. 1989, ApJS, 71, 623
Carlsson, M., & Judge, P. G. 1993, ApJ, 402, 344
Carpenter, K. G., Pesce, J. E., Stencel, R. E., Brown, A., Johansson, S., & Wing, R. F. 1988, ApJS, 68, 345
Carpenter, K. G., Robinson, R. D., Wahlgren, G. M., Ake, T. B., Ebbets, D. C., Linsky, J. L., Brown, A., & Walter, F. M. 1991, ApJ, 377, L45
Cassatella, A., & Harris, A. W. 1983, NASA *IUE* Newsletter, No. 23, 21
Cassatella, A., Ponz, D., & Selvelli, P. L. 1983, NASA *IUE* Newsletter, No. 21, 46
Cuntz, M., & Stencel, R. E. 1991, in Mechanics of Chromospheric and Coronal Heating, ed. P. Ulmschneider, E. R. Priest, & R. Rosner (Berlin: Springer), 206
Dupree, A. K. 1991, in Mechanics of Chromospheric and Coronal Heating, ed. P. Ulmschneider, E. R. Priest, & R. Rosner (Berlin: Springer), 185
Eaton, J. A., & Johnson, H. R. 1988, ApJ, 325, 355
Eaton, J. A., Johnson, H. R., & Cadmus, R. R. 1990, ApJ, 364, 259
Eriksson, K., Gustafsson, B., Johnson, H. R., Querci, F., Querci, M., Baumert, J. H., Carlsson, M., & Olofsson, H. 1986, A&A, 161, 305
Evans, N. R., & Imhoff, C. L. 1985, NASA *IUE* Newsletter, no. 28, 77
Field, G. B., & Steigman, G. 1971, ApJ, 166, 59
Fleischer, A. J., Gauger, A., & Sedlmayr, E. 1992, A&A, 266, 321
Gayley, K. G. 1992, ApJS, 78, 549
Haisch, B. M., Linsky, J. L., Weinstein, A., & Shine, R. A. 1977, ApJ, 214, 785
Hartmann, L., & Avrett, E. H. 1984, ApJ, 284, 238
Henry, G., & Baliunas, S. L. 1992, private communication
Hoffleit, D. 1982, The Bright Star Catalogue (New Haven: Yale Univ. Obs.)
Hubený, I. 1985, A&A, 145, 461
Jaksha, D. 1989, private communication
Johnson, H. R. 1974, NCAR Tech. Note, No. STR-95
———. 1991, A&A, 249, 455
Jørgensen, U. G., & Johnson, H. R. 1991, A&A, 244, 462
Judge, P. G. 1986a, MNRAS, 221, 119
———. 1986b, MNRAS, 223, 239
———. 1990, ApJ, 348, 279
Judge, P. G., Carpenter, K. G., & Harper, G. M. 1991, MNRAS, 253, 123
Judge, P. G., & Stencel, R. E. 1991, ApJ, 371, 357
Kelch, W. L., Linsky, J. L., Basri, G. S., Chiu, H-Y, Chang, S-H, Maran, S. P., & Furenlid, I. 1978, ApJ, 220, 962
Kukarkin, B. V., et al. 1976, General Catalog of Variable Stars, 3rd Supplement (3d ed.; Moscow: Akad. Nauk)
Kurucz, R. L., & Peytremann, E. 1975, Smithsonian Astrophys. Obs. Rep., No. 362
Lennon, D. J., Dufton, P. L., Hibbert, A., & Kingston, A. E. 1985, ApJ, 294, 200
Luttermoser, D. G. 1988, Ph.D. thesis, Indiana Univ.
———. 1993, in preparation
Luttermoser, D. G., Bowen, G. H., Willson, L. A., & Brugel, E. W. 1993, in preparation
Luttermoser, D. G., & Johnson, H. R. 1992, ApJ, 388, 579
Luttermoser, D. G., Johnson, H. R., Avrett, E. H., & Loeser, R. 1989, ApJ, 345, 543
Malagnini, M. L., Morossi, C., Buser, R., & Parthasarathy, M. 1992, A&A, 261, 558
Middlekoop, F. 1982, A&A, 113, 1
Olnon, F. M., & Raimond, E. 1986, A&AS, 65, 607
Phillips, M. M. 1979, ApJS, 39, 377
Plez, B., Brett, J. M., & Nordlund, Å. 1992, A&A, 256, 551
Rutten, R. G. M. 1987, A&A, 177, 131
Scargle, J. D., & Strecker, D. W. 1979, ApJ, 228, 838
Schrijver, C. J. 1987, A&A, 172, 111
Smith, V. V., & Lambert, D. L. 1985, ApJ, 294, 326
Stencel, R. E., Carpenter, K. G., & Hagen, W. 1986, ApJ, 308, 859
Stencel, R. E., Linsky, J. L., Brown, A., Jordan, C., Carpenter, K. G., Wing, R. F., & Czyzak, S. 1981, MNRAS, 196, 47P
Stencel, R. E., & Mullan, D. J. 1980, ApJ, 238, 221
Stencel, R. E., Mullan, D. J., Linsky, J. L., Basri, G. S., & Worden, S. P. 1980, ApJS, 44, 383
Tsuji, T. 1988, A&A, 197, 185
———. 1991, A&A, 245, 203
Ulmschneider, P. 1991, in Mechanics of Chromospheric and Coronal Heating, ed. P. Ulmschneider, E. R. Priest, & R. Rosner (Berlin: Springer), 328
Vernazza, J. E., Avrett, E. H., and Loeser, R. 1973, ApJ, 184, 605 (VAL I)
———. 1976, ApJS, 30, 1 (VAL II)
———. 1981, ApJS, 45, 635 (VAL III)
Wannier, P. G., & Sahai, R. 1986, ApJ, 311, 335
Wiedemann, G., & Ayres, T. R. 1991, ApJ, 366, 277